NATIONAL AERONAUTICS AND SPACE ADMINISTRATION

Technical Report No. 32-975

Radiation Measurement Techniques

Wesley A. Menard
George M. Thomas

JET PROPULSION LABORATORY
CALIFORNIA INSTITUTE OF TECHNOLOGY
PASADENA, CALIFORNIA

August 1, 1966

NATIONAL AERONAUTICS AND SPACE ADMINISTRATION

Technical Report No. 32-975

Radiation Measurement Techniques

Wesley A. Menard
George M. Thomas

E. Laumann, *Manager*
Aerodynamic Facilities Section

JET PROPULSION LABORATORY
CALIFORNIA INSTITUTE OF TECHNOLOGY
PASADENA, CALIFORNIA

August 1, 1966

Prepared Under Contract No. NAS 7-100
National Aeronautics & Space Administration

CONTENTS

FIGURES

FIGURES (Cont'd)

33771

ABSTRACT

This Report describes quantitative radiation measurement techniques developed for use in an electric arc-driven shock tube. Shock layer radiance in the 0.3 to 2.7 μ region is measured using a carbon-coated thin film gage. The methods of calibrating the gage and of relating the gage response to the gas intensity are described. Two techniques for measuring the shock layer thickness are presented. The effects of shock wave attenuation and radiation from sources outside the shock layer are shown to be important in certain thermochemical regimes. Prism and grating monochromators have been adapted to the shock tube and used to measure spectral radiation in the 2000–10,000 Å region, with resolution as high as 1Å. The methods described have been applied in experimental studies of oscillator strengths, and nonequilibrium and equilibrium radiation. Absolute intensity measurements of the cyanogen violet band system produced in a carbon arc calibration source are also presented. In the ultraviolet region of the spectrum, stray light interference is a common problem. Techniques to eliminate the stray light such as using filters, fluorescent coatings, and solar blind detectors are discussed.

I. INTRODUCTION

The purpose of this Report is to present the laboratory techniques developed at Jet Propulsion Laboratory (JPL) for studying the gaseous radiation produced in a hypervelocity shock tube. These techniques have been used in a recent investigation of the radiation from planetary atmospheres (Ref. 1). To make measurements in a high performance shock tube, such as the JPL electrically driven facility (Ref. 2), an important requirement of the instrumentation is fast response time. To meet this requirement, all radiation instruments to be described here were designed for response times of the order of 1 μsec or less.

In the first section, a gage for measuring the total stagnation point radiation to a shock tube model and the method by which it is calibrated are described. The gage is a platinum film coated with a thin layer of carbon. To isolate the gage from the hot gas and measure radiation alone, the gage is mounted behind a window in the model. The gage measures heat transfer; and, to

obtain the gas intensity, a measurement of shock standoff distance is required. Techniques for measuring shock standoff distance are presented. Finally, an analysis is made of the effects that shock wave attenuation and radiation from sources outside the shock layer have on the gage measurements.

In the second section, methods are presented for measuring spectral radiation from shock heated gases in the region 2000–10,000 Å. Prism and grating monochromators equipped with sensitive photomultipliers are described. Calibration techniques and data reduction procedures are presented. The carbon arc as a calibration source is discussed and the plasma CN intensity is measured. Spectrograms of the CN violet band system, showing much of the rotational line structure, were also obtained. Some of the problems involved in eliminating stray light for measurements in the ultraviolet (UV) spectral region are discussed.

II. TOTAL RADIATION

A. Total Radiation Gage

A gage has been developed for measuring the total equilibrium radiation to the stagnation point of a shock tube model. Because this gage has been described in detail previously (Ref. 3), only a general description will be given here. The gage consists of a thin-film platinum resistance thermometer coated with a thin film of carbon. The gage is mounted behind a pyrex window in a flat-faced cylinder model shown schematically in Fig. 1. Radiant energy from the shock layer strikes the carbon covering of the resistance gage and

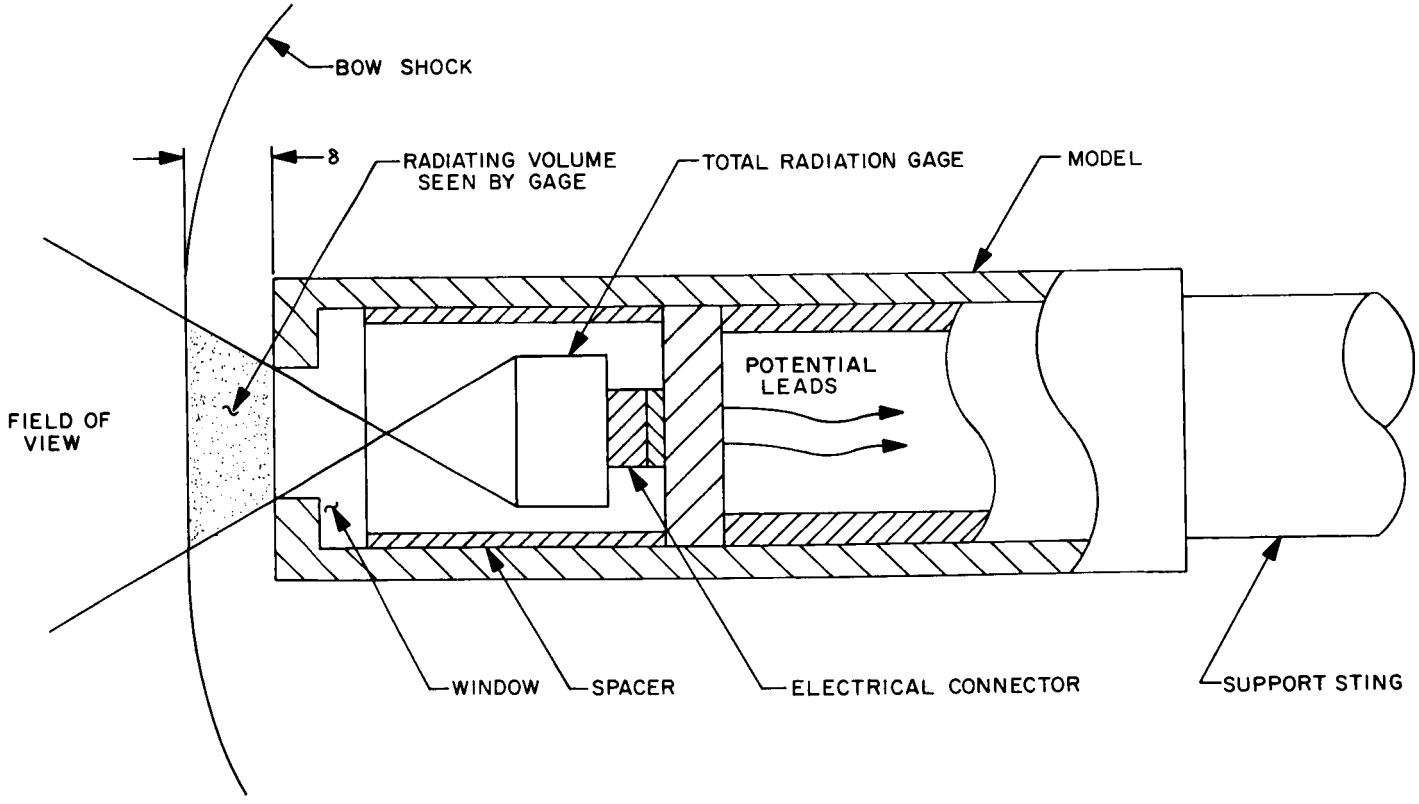

Fig. 1. Schematic of total radiation gage and model

the energy is transformed into heat. The resistance gage then responds to the temperature rise of its backing material.

Two requirements of the high absorbing carbon film are (1) that its absorptance not vary with wavelength over the wavelength region of interest, and (2) that it be thin enough to allow rapid diffusion of heat to the sensing element in order not to seriously affect the gage response time. An evaporated carbon film of uniform thickness less than 1 μ was prepared and mounted over a platinum-sputtered sample. The sample was tested for spectral reflectance in the wavelength region of 0.2 to 2.7 μ. The measurements in the form of absorptance are presented in Fig. 2. For comparison, the absorptance of an uncoated, opaque, platinum film is also presented. In the ultraviolet and visible regions of the spectrum, the carbon absorptance is nearly constant at 0.80; but in the infrared region, the absorptance varies from this mean value by $\pm 20\%$. If the bulk of the radiation being measured lies below 0.6 μ, such as in the case of planetary atmospheres (Ref. 1), there is little error in assuming the absorptance to be constant from 0.2 to 2.7 μ. The wavelength coverage in practice, however, has been determined by the transmission of the window. For the case of a pyrex window, the wavelength range of the gage is about 0.3 to 2.7 μ. The response time of the gage has been shown to be on the order of 2 μsec (Ref. 3).

A photograph of the gage is shown in Fig. 3. The gage element was prepared by sputtering a thin film of platinum (0.035 × 0.75 in.) upon a quartz backing

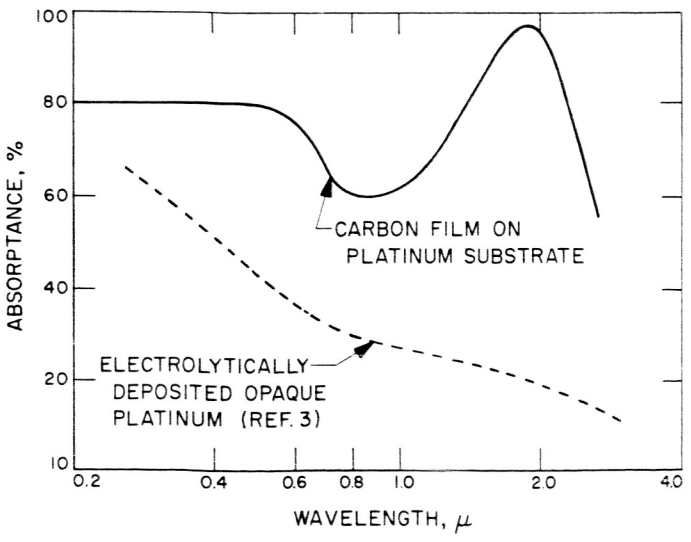

Fig. 2. Spectral absorptance of carbon coated total radiation gage

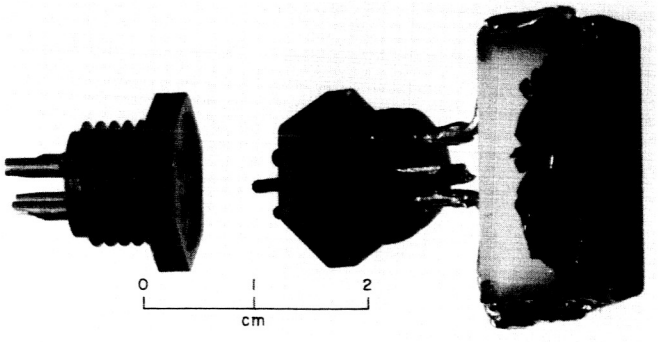

Fig. 3. Total radiation gage

material, and heat-treating to bond the two materials at the interface. The approximate thickness of the platinum for a typical gage, having a resistance of 200 ohms, was calculated to be 0.01 μ from the following equation

$$T = \frac{\rho}{R}\frac{l}{W} \tag{1}$$

where ρ is the resistivity of the platinum, R is the resistance, l is the length of the gage, and W is the width.

Two methods have been used to prepare the carbon coating. One method employs an evaporation technique, as described in Ref. 3. By this procedure, the carbon is evaporated onto a microscope slide and then transferred to the gage. In the other method, carbon from a spectroscopic rod is sputtered directly onto the gage. It has been found by comparing theoretical and experimental response times (Ref. 3) that carbon films prepared by either procedure make good thermal contact with the platinum film. A good mechanical bond between the carbon and platinum is more easily obtained, however, in the sputtering technique.

The electrical circuit for the gage is shown in Fig. 4. Power is supplied to the circuit by a 200 v dc power

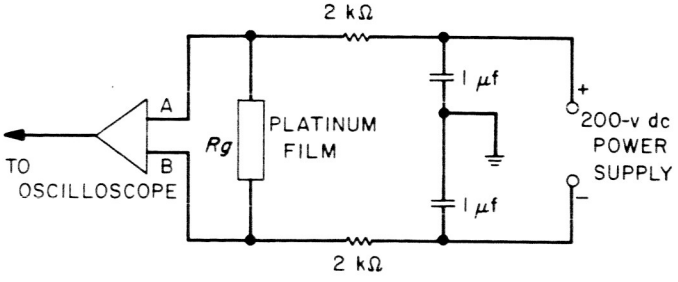

Fig. 4. Schematic of total radiation gage circuit

supply. The current limiting resistors are chosen large in comparison with the gage resistance R to maintain a constant current in the gage circuit. The gage output-voltage leads are connected to a differential preamplifier (Tektronix Type D) to eliminate circuit noise that is common to both leads. The output of the amplifier is displayed on an oscilloscope.

To make the gage measurement quantitative, the gage response must be related to the intensity of the radiative source. The geometry of the problem is illustrated in Fig. 5 for the case of a plane parallel gas layer. The gage is isolated from the gas by a window. For a transparent and isotropic radiating gas volume, the radiant power (watts) reaching a differential element dA_i of the detector surface is given by

$$dq_i dA_i = \tau G_\lambda d\lambda dV\left(\frac{dA_i \cos\theta}{S_i^2}\right) \tag{2}$$

where $G_\lambda d\lambda$ is the rate of energy emitted from the volume element dV per unit solid angle in the wavelength interval λ to $\lambda + d\lambda$, τ is the spectral transmission

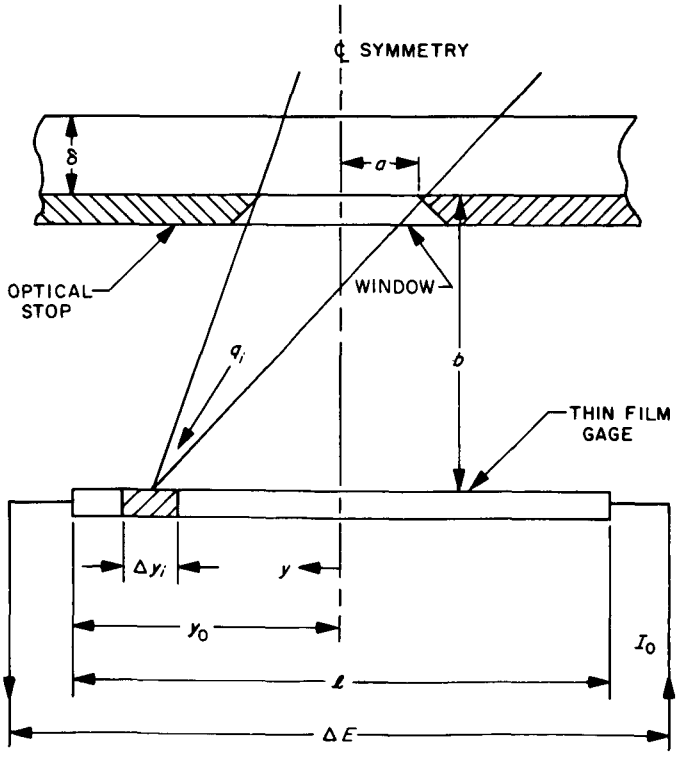

Fig. 5. Theoretical model for relating the gage response to the heat transfer distribution along the gage surface

of a window located between the volume element and the detector surface, and the quantity in parenthesis is the solid angle. The heat transfer to the area dA_i from the entire volume seen by the elemental area is thus

$$q_i = \tau \frac{G}{4\pi} f_i(y) \tag{3}$$

where

$$f_i(y) = \int \frac{dV \cos\theta}{S_i^2}$$

$G = 4\pi \int G_\lambda d\lambda$ is the gas intensity per unit path length (w/cm^3).

If we assume that the heat flow remains one-dimensional for each differential element of the gage surface, the solution of the one-dimensional heat conduction equation may be applied to each element to relate the heat transfer to the temperature rise of the gage element:

$$\Delta T_i = \frac{2}{\beta}(t)^{1/2} q_i H \tag{4}$$

where H is the absorptance of the gage, $\beta = (\pi\rho ck)^{1/2}$ is a thermal material property of the quartz backing material, and t is the time. The voltage change of the element is related to ΔT_i as follows:

$$\Delta E_i = I_0 \alpha \frac{R_0}{l} \Delta T_i \Delta y_i \tag{5}$$

where I_0 is the current flowing through the gage, R/l is the gage resistance per unit length, Δy_i is the element length, and α is the temperature coefficient of resistance of the gage material.

The total voltage change for all elements of the gage is then given by

$$\Delta E = \sum_i \Delta E_i \tag{6}$$

When Eqs. (3) through (6) are combined, the following expression is obtained:

$$G = \frac{\Delta E}{(t)^{1/2}}\left[\frac{\tau H E_0 \Phi}{l\pi}\int_0^{y_0} f_i(y)\, dy\right]^{-1} \tag{7}$$

where $\Phi = \alpha/\beta$ and $E_0 = I_0 R_0$

The window transmission τ is obtained from simple photometric measurements and the absorption measurements have been described previously. The values of l and E_0 are obtained in a straightforward manner. The term accounting for the geometry, $\int f_i(y)\,dy$, is obtained by numerical integration and is found (Ref. 3) to result in the distribution illustrated in Fig. 6. The quantity Φ is determined in the following way: The gage response for a constant amplitude heat pulse Q is given by

$$\frac{\Delta E}{(t)^{1/2}} = 2QE_0\Phi \tag{8}$$

Thus, the lumped constant Φ is obtained most simply by Joule heating the gage with a constant amplitude current pulse and observing the gage response. For a constant heating current the Joule heat is given by

$$Q = \frac{I_0^2 R_0}{A_g} \tag{9}$$

where I_0 is the current and A_g is the gage area. Combining Eqs. (8) and (9) we obtain with $E_0 = I_0 R_0$:

$$\Phi = \frac{[\Delta E/(t)^{1/2}]\,A_g}{2I_0^3 R_0^2} \tag{10}$$

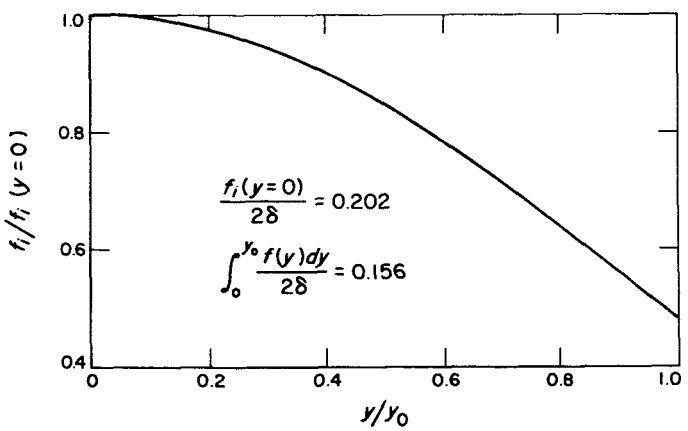

Fig. 6. View factor for the experimental geometry: $a = 0.759$ cm; $b = 2.11$ cm; and $y_0 = 0.953$ cm

Equation (10) shows that large errors can occur if the current pulse amplitude is not maintained constant to a high degree of accuracy. Figure 7 shows a circuit that has been developed at JPL which limits the current droop to about ½% of I_0. It consists of essentially four elements: (1) a Tektronix 555 oscilloscope, (2) a power supply, (3) a pulse amplifier, and (4) a constant voltage bridge. The plus gate from the oscilloscope provides a convenient pulse source of extremely fast rise time (less than 0.01 μsec). The measurement of R_0 is done accurately, using standard bridge balancing techniques. The measurement of gage area is possibly the largest source of error for this technique. The sputtered-platinum film area is measured most accurately for films of large dimensions. An oscillogram of the current pulse and parabolic gage response predicted by Eq. (10) is shown in Fig. 8. The time history of the gage voltage is measured from the oscillogram and plotted as shown in Fig. 9. The slope of the straight line in Fig. 9 determines $\Delta E/(t)^{1/2}$ in Eq. (10). The current pulse I_0 is determined by developing a voltage across a 10-ohm standard resistor which is equal to a known bucking voltage supplied by the Type Z preamplifier. The top of the current pulse is recorded on the oscillogram as a permanent record of the current droop. Equation (10) may then be solved for the calibration constant, Φ. For gages ranging in resistance from 100–400 ohms, we have obtained Φ values from 0.007–0.008 $cm^2/w(sec)^{1/2}$. This data compares favorably with values quoted in the literature (Ref. 4) for much lower resistance gages.

The total radiation gage has been used to measure stagnation point heating and shock layer radiance on a flat-faced cylinder model (Ref. 1), in an arc-heated shock tube. The gage was mounted in the model as illustrated in Fig. 1. A photograph of the model is presented in Fig. 10. The model was supported by a sting along the shock tube centerline facing the oncoming shock wave. In a few μsec after the incident shock passed the model, a bow shock was formed and a steady constant thickness layer of gas behind the bow shock was viewed by the gage. The test time was terminated by the arrival of the contact surface. A typical trace of the gage response is presented in Fig. 11. The slight bump on the trace indicates arrival of the incident shock. The formation of the bow shock requires approximately 4 μsec, after which a parabolic response of the gage begins. Also shown on the oscillogram is the output of a photomultiplier viewing the test gas ahead of the bow shock. The smoothness of the gage response is indicative of the high signal to noise ratio of the gage and circuitry.

The gage sensitivity has not been a limiting factor in our experiments. For the lowest as well as the highest heating rates applied to the gage, the signal to noise ratio remained large and the response remained parabolic. The only limit encountered at low heating rates was the inability to amplify the signal on the oscilloscope so that accurate measurements of ΔE could be made.

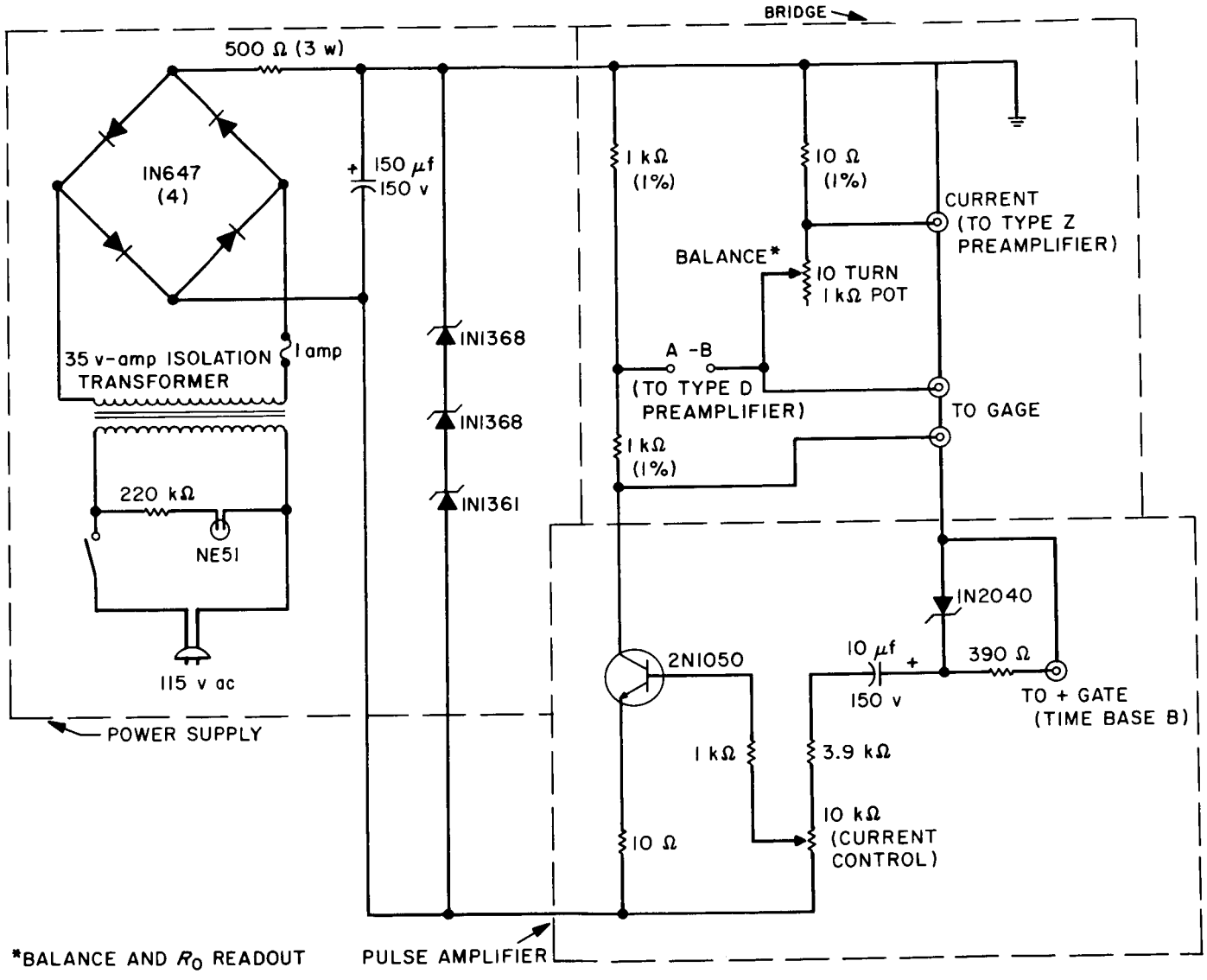

Fig. 7. Total radiation gage calibration circuit

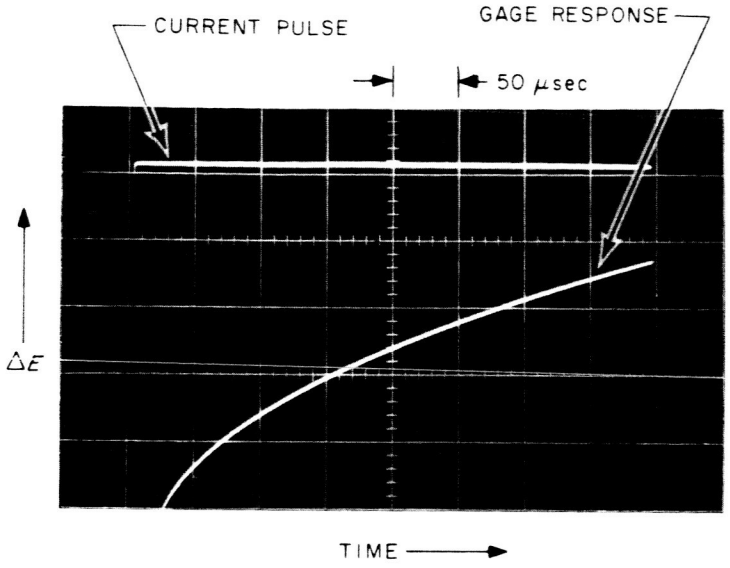

Fig. 8. Oscillogram showing radiation gage response to a constant amplitude heat pulse

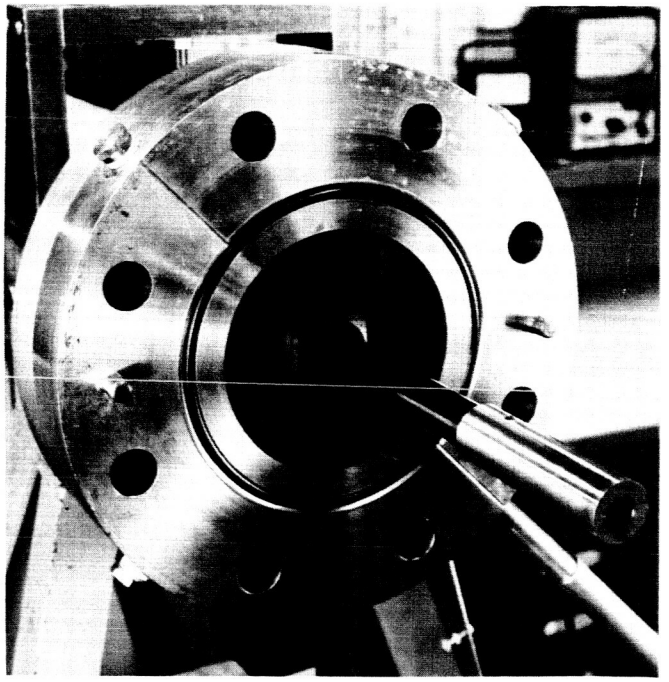

Fig. 10. Photograph of shock tube model used for stagnation point radiative heat transfer measurements

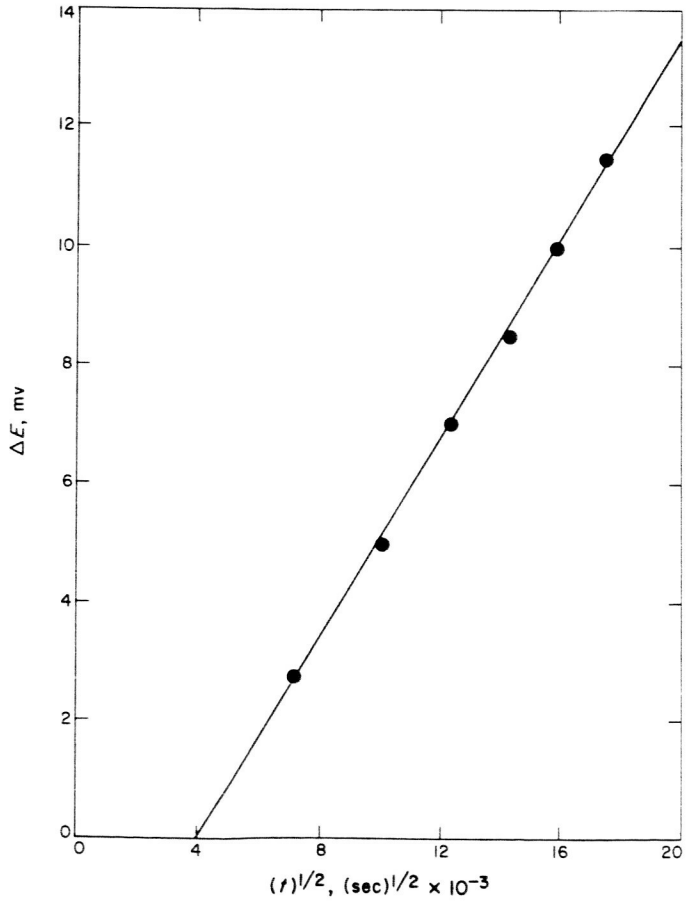

Fig. 9. Typical gage calibration results

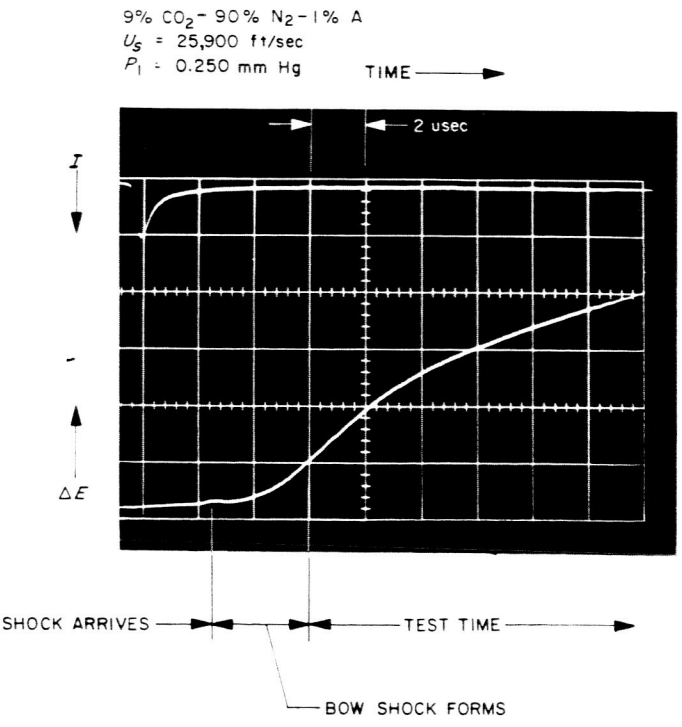

Fig. 11. Oscilloscope trace showing response of the stagnation point total radiation gage

B. Shock Standoff Distance

To evaluate the geometrical view factor for the gage requires the shock standoff distance, δ. The standoff distance was measured using an STL image converter camera and a rapid shutter technique.

A photograph from the image converter camera is shown in Fig. 12(a). The camera views the gas through the wall of a one-foot-long glass test section. The model is the 1¼-in. flat-faced cylinder and the test condition was shock velocity of 28,000 ft/sec in a 0.25 mm Hg mixture of 9% CO_2–90% N_2–1% A. The camera has insufficient resolution for measuring the standoff distance accurately, so it was necessary to enlarge the photograph for more accurate measurements. By this technique, the uncertainty in the δ measurement was about 25%.

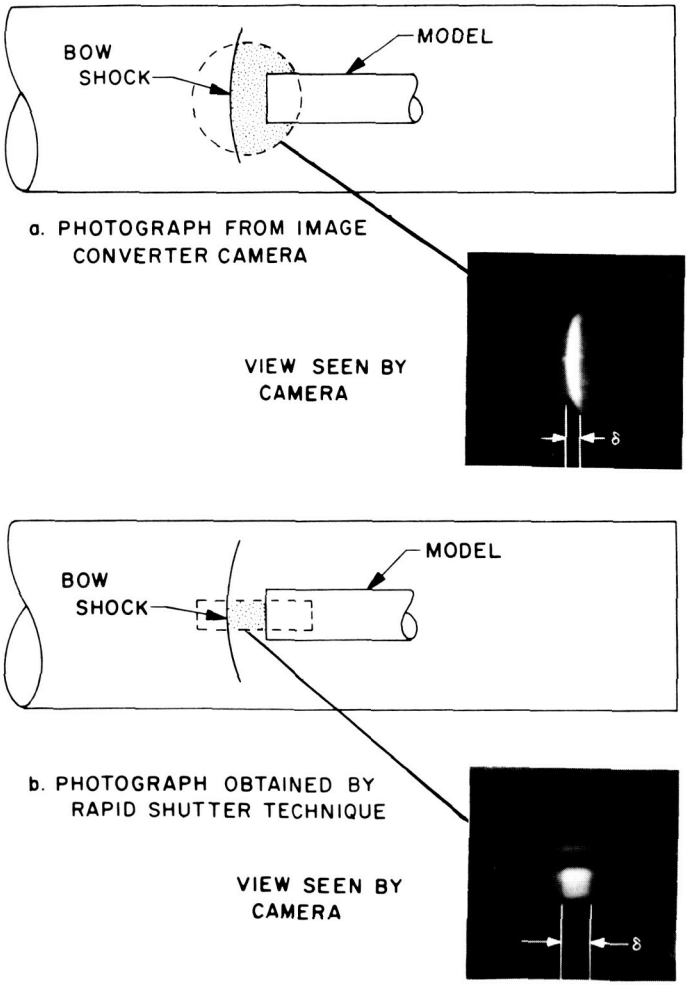

Fig. 12. Shock standoff measurements on a 1¼-in. flat-faced cylinder model. Top photograph (a) taken with an image converter camera. Bottom photograph (b) obtained using the rapid shutter. Photographs do not have the same magnification

In Fig. 13, a more accurate photographic technique is illustrated. An electromechanical shutter of the type designed by Camm (Ref. 5) was used to obtain photographs of the standoff distance through a slit and window in the shock tube sidewall. The shutter has an open and close time of approximately 30 μsec.

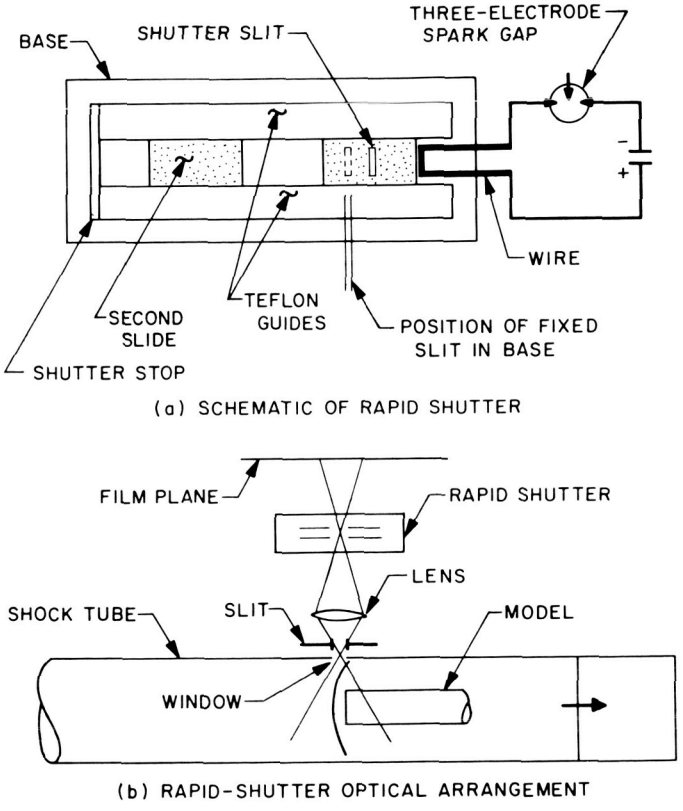

Fig. 13. The rapid shutter. Top: Schematic of rapid shutter mechanism. Bottom: Schematic showing how standoff distance measurements were made in the shock tube

The shutter consists of a thin rectangular slide of micarta with a slit at the center, which rides in V-grooves milled into Teflon guides. The slit, about 50 μ wide, is formed by cementing thin shim-stock over a hole in the micarta. Before the firing takes place, the shutter rests against the end of an 0.040-in.-dia nichrome wire which is peened flat to give good surface contact with the shutter. The Teflon guides are fastened to a metal base containing a 50-μ fixed slit. A 14.5-μf capacitor charged to 7.5 kv and in series with an electrode spark gap is

connected across the ends of the nichrome wire. In operation, a high voltage trigger pulse is sent to the trigger electrode of the spark gap and breaks down the gap, discharging the capacitor through the resistance of the nichrome wire. The wire is heated to a high temperature in a few μsec and undergoes thermal expansion, imparting an impulse movement to the shutter. The motion of the moving shutter is stopped by momentum exchange when it collides with a second slide located nearby and the resulting motion of the slide is, in turn, stopped by an inelastic collision with a stop covered with soft damping material.

The optical system for photographing the shock layer contains a lens which focuses objects at the shock tube centerline on the film plane with 1 to 1 magnification. The slits are arranged with their longest dimension in the direction of the shock tube axis, with the shutter slit moving transverse to the shock tube. The shutter is triggered approximately 100 μsec prior to arrival of the incident shock by a photomultiplier upstream of the measuring station. After an inherent fixed delay of 80 μsec, the shutter opens and closes, exposing the film to the luminosity of the shock layer in front of the model. A photograph of the shock layer in front of the flat-faced cylinder model is shown in Fig. 12(b). The gas was 9% CO_2–90% N_2–1% A, and the shock speed was 28,500 ft/sec. The standoff distance could be measured to within 0.1 mm, or an accuracy of 1% for this model. The results were within 6% of Vinokur's prediction (Ref. 6) in this case.

C. Contribution from Sources Outside the Shock Layer

The gage measures all radiation lying in its field of view. Therefore, the contribution of sources outside the shock layer must be considered in interpreting the measurement. These sources include the test slug gas lying between the model and the contact surface, as well as the hot driver gas upstream of the contact surface.

The ratio of the heat transfer to the gage from the stagnation region, q_3, to the heat transfer from the test slug gas, q_2, is given approximately by

$$\frac{q_3}{q_2} = \frac{G_3\,\delta}{G_2 L\,(t)} \tag{11}$$

where δ is the standoff distance, $L\,(t)$ is the distance from the model face to the contact surface, and G_2 and G_3 are the gas intensities per unit path length of the test slug and shock layer gas, respectively. The total heat transfer q_t to the gage is the sum of the two:

$$q_t = q_2 + q_3 \tag{12}$$

The measured heat transfer q_t, therefore, exceeds the desired heat transfer q_3 by the ratio:

$$\frac{q_t}{q_3} = 1 + \frac{G_2 L\,(t)}{G_3 \delta} \tag{13}$$

The length $L\,(t)$ may be approximated by the equation:

$$L\,(t) = U_s\, t_{max}\left(1 - \frac{t}{t_{max}}\right) \tag{14}$$

where U_s is the shock velocity, t_{max} is the total test time, and t is the time after the arrival of the shock at the model nose. Equations (13) and (14) show that this source of error decreases linearly with time and depends also on the ratio of the intensities G_2 and G_3. To evaluate this effect, independent intensity measurements (such as the spectral measurements to be described later) or a theoretical prediction of the intensity as a function of the gas and its thermochemical state must be available.

The results of this calculation are presented in Fig. 14 for a planetary gas mixture consisting of 30% CO_2 and 70% N_2. The intensities were obtained from the predictions of Spiegel and Wolf.[1] The ratio q_t/q_3 given by Eq. (13) is plotted as a function of shock speed for test times of 10 and 20 μsec. At about 28,000 ft/sec the correction is negligible. We have not made measurements at 23,000 ft/sec; however, the effect should be observed as a decrease in measured intensity with time in the oscillogram records.

The driver gas contribution to the signal is more difficult to predict since this radiation is due to impurities near the contact surface in an arc-driven shock tube. If this radiation is assumed confined to a constant thickness slug moving at constant velocity, the gage will sense a constant heating rate after the slug enters its field of view and the effect will not be separated from the shock layer contribution. However, this source should be seen on the oscillogram prior to the arrival of the incident shock at the model face. This effect has been observed as a slight rise in the gage signal for lower shock velocities but has not been observed at incident shock velocities above about 20,000 ft/sec. It was concluded

[1]Personal communication from J. M. Spiegel and F. Wolf, JPL, February 1964.

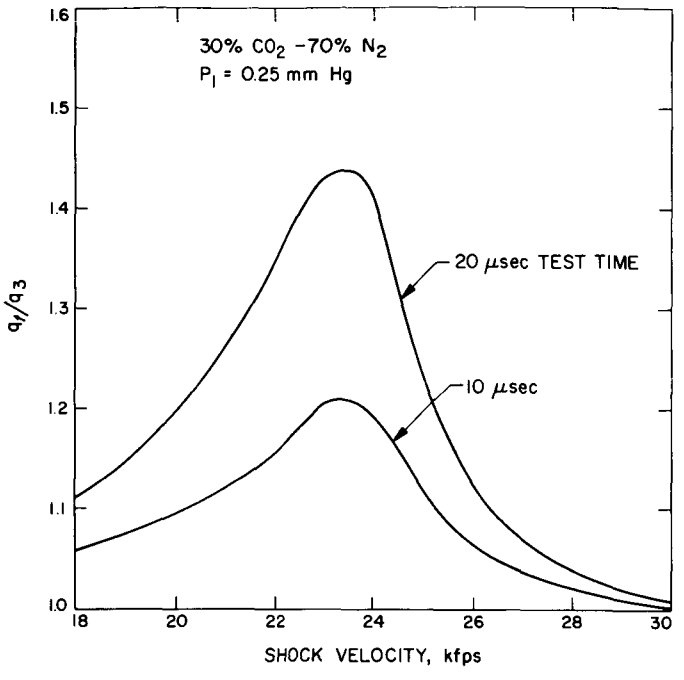

Fig. 14. Effect of test gas radiation on the total gage measurements. Curves calculated from Eq. (13) for $t = 0$

that the error due to these sources should be measured for each experimental condition and is not negligible for some thermochemical regimes depending upon the test gas.

Another effect which has been investigated is the contribution of the nonequilibrium shock front to the measurement. This effect requires the experimental measurement of the nonequilibrium radiation relaxation distance and quantitative nonequilibrium intensity measurements. For simulated planetary atmospheres (CO_2–N_2 mixtures), the nonequilibrium intensities have been found (Ref. 1) to exceed that in the earth's atmosphere by as much as a factor of 4 at the same flight velocity. The nonequilibrium contribution to the measurement will be correspondingly greater in this case. The relaxation distances are also about a factor of 3 greater than for air and will represent a larger fraction of the standoff distance on a given model. For the 1.25-in.-dia flat-faced cylinder model used in our studies, the relaxation distance is less than 1% of the standoff distance and the nonequilibrium contribution was estimated to be negligible. The nonequilibrium contribution depends largely on the size of the model. For example, the shock layer of a small hemispherical 5-mm nose radius ballistic range model would have a nonequilibrium relaxation distance nearly equal to the standoff distance for a flight velocity of 20,000 ft/sec and freestream pressure less than about 15 mm Hg.

Shock wave attenuation is another effect which has been considered in interpreting our stagnation point measurements. For a 40-ft-long driven tube on the 6-in. arc-heated shock tube, the attenuation is about 2,000 ft/sec over the length of the tube for shock velocities in the range of 20,000–30,000 ft/sec. This velocity increment will theoretically cause large gradients in the thermodynamic state of the test gas. For this reason, the radiation from the gas behind the bow shock has been monitored photometrically. The results indicate that an approximately constant temperature is maintained in the shock layer on a large number of runs when the test gas is air and shock velocities are above 25,000 ft/sec. However, on other runs the assumption of a constant temperature in the shock layer is clearly untenable from the measurements. An increase of the radiation by a factor of 2 during the test time is not uncommon. These "bad runs" appear to occur at random. The reason for this random performance of the shock tube has not been explained. The measured shock attenuation on these runs is about the same as for "good runs" where the temperature remains constant. This phenomenon requires further study; however, the test gas at the nose of the model clearly needs to be monitored on each run.

III. SPECTRAL RADIATION

In addition to total radiation measurements, spectral measurements have been made for identification of radiating species and determination of electronic oscillator strengths. Spectral measurements have also been used for studying nonequilibrium and equilibrium radiation in planetary atmospheres (Ref. 1). The excitation and relaxation processes of various species produced behind shock waves have also been studied spectrally. From the spectrum of shock heated gas the dominant radiative species are identified. From intensity measurements of the vibrational transitions of molecular bands, it has been possible to determine electronic oscillator strengths (Ref. 1). A typical spectrum of the radiation from a planetary gas mixture is shown in Fig. 15. The dominant radiator is seen to be the violet band system ($B^2\Sigma \rightarrow X^2\Sigma$) of the CN molecule.

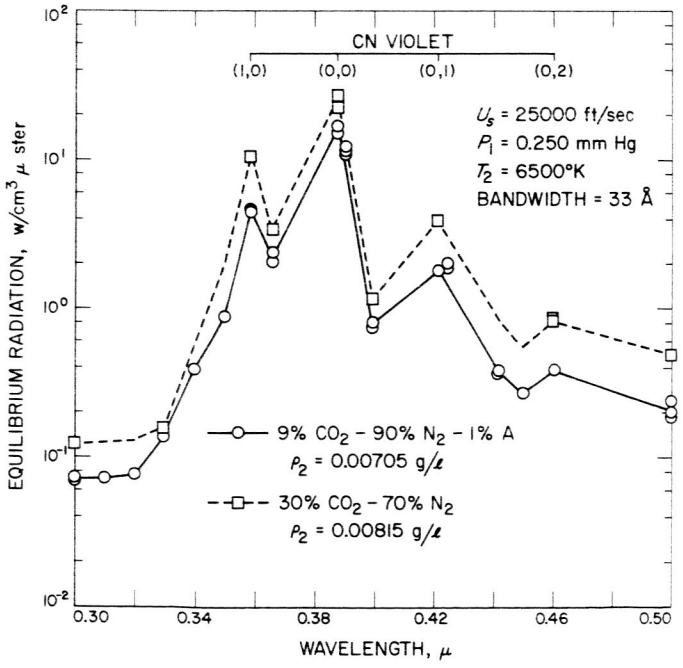

Fig. 15. Typical spectral radiation results, taken from Ref. 1

Spectral measurements such as shown in Fig. 15 are obtained from monochromators equipped with multiplier phototubes. The monochromator disperses the radiant energy from the shock tube into a spectrum. The dispersing element may be either a prism or a diffraction grating. The choice of whether to use a prism or a grating depends upon the application. It is often desirable because of transmission losses through a prism, to use a grating when observing sources of low intensity or working in the ultraviolet. The grating has, in general, a considerable advantage in resolving power. Gratings also produce a linear dispersion of the spectrum at the focal plane of the monochromator, while the dispersion of a prism varies with wavelength, becoming poorer as wavelength increases. Overlapping of the various orders is a disadvantage of the grating monochromator. Stray light interference from the grating can also cause a serious problem in the ultraviolet region, as is discussed later.

A. Experimental Apparatus

Three Perkin–Elmer Model 98 quartz prism monochromators have been used for low resolution (50–400 Å band pass) work in the spectral region from 4000–10,000 Å. For resolution of about 30 Å in the 3000–5000 Å region, a Bausch and Lomb ½-meter-grating monochromator has been used. To obtain higher resolution and to extend the wavelength coverage down to about 2000 Å, a Jarrell–Ash $f/6.3$ spectrograph has been fitted with adjustable exit slits along the focal plane. This modification allows the band pass to vary from 100 Å to about 1 Å. Six photomultipliers mounted behind the exit slits allow six channels of spectral data to be obtained from one shock tube run. In Fig. 16, a photograph of the exit compartment of

Fig. 16. Exit compartment of modified Jarrell–Ash monochromator

the monochromator is presented. To obtain good response time requires a low RC time constant in the photomultiplier circuitry. For this reason and because of the limited space in the exit compartment, the circuitry was miniaturized and packaged in the tube holders.

Figure 17 shows a schematic of the optical arrangement of the various monochromators with respect to the shock tube. The prism instruments are arranged to view the radiation from a single shock tube port. Radiant energy leaving the shock tube slit is collected by a quartz lens which sends a collimated beam to the pyrex beam splitter. The light is split into three beams and focused on the monochromator entrance slits by lenses. The grating instruments are arranged in such a way that radiation from the shock tube slit is focused by a single suprasil lens directly onto the monochromator entrance slit. Suprasil is used to obtain transmission down to 2000 Å.

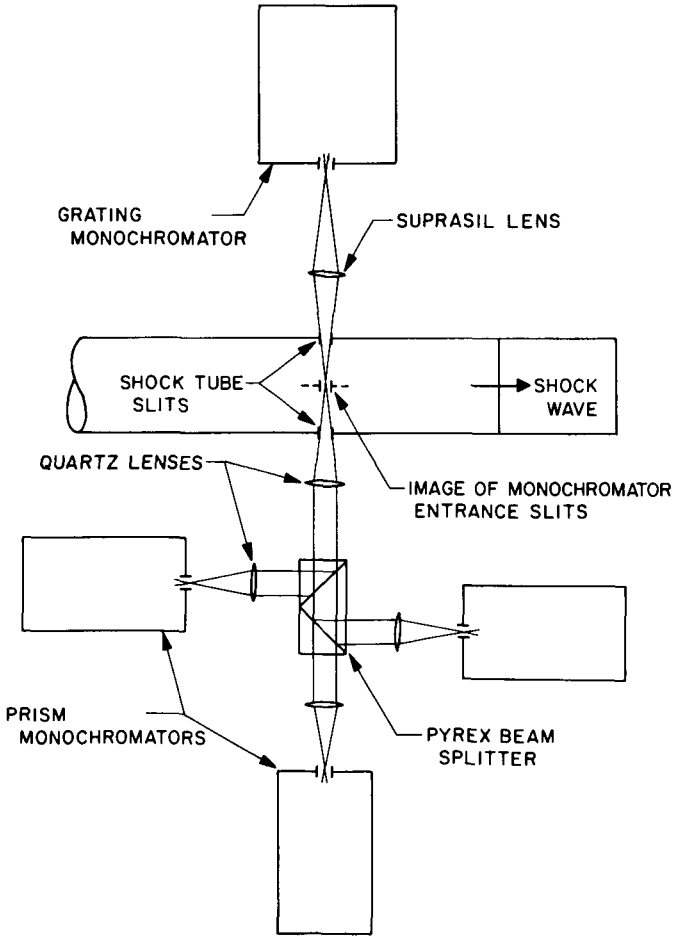

Fig. 17. Optical arrangement of the prism and grating monochromators with the shock tube

The time response of the optical system used for obtaining photometric measurements is given by

$$t = \frac{X}{U_s} \tag{15}$$

where X is the width of the monochromator field of view within the shock tube, and U_s is the shock velocity. If small slit widths and appropriate magnification of the optical system are used, response times less than 0.1 μsec are obtainable.

To cover the spectral range from 10,000–2000 Å, three different photomultipliers have been used. An RCA 7102 photomultiplier, which has peak response in the near infrared, is used in the region from 10,000–6000 Å. In the region from 6500–3000 Å, an RCA 1P28 photomultiplier is used. And below 3000 Å, an EMR 541F-05M photomultiplier is used. The EMR tube is discussed further in Section III-E. The 1P28 photomultiplier circuit is shown in Fig. 18. Large divider resistors are used across the dynodes and the supply voltage is varied from 700–1200 v to allow flexibility in gain. Capacitors across the last few dynode stages help to eliminate nonlinearity effects. The photomultiplier output is amplified by a Type L plug-in preamplifier, and the signal is recorded by means of a Tektronix Type 555 oscilloscope and Polaroid film camera. To obtain sufficient rise time the effective capacitance of the circuitry is lowered by means of an emitter follower. The emitter follower shown in Fig. 18 provides a net electrical time constant better than 0.04 μsec.

B. Calibration Techniques

Wavelength calibration is accomplished by the identification of lines from a known light source. For this purpose we have used mercury, sodium, thallium, and argon lamps. The dispersion is measured by taking a spectrogram of the light source and measuring the separation distance between the known lines. The reciprocal linear dispersion is the ratio of the wavelength separation of two close spectral lines to their actual separation distance in the dispersed spectrum. The order I dispersion of one of the Jarrell–Ash gratings is shown in Fig. 19. Spectrograms were obtained with a Polaroid camera at the exit plane of the instrument, using a Hg light source. The reciprocal linear dispersion is seen to be about 10 Å/mm at 3000 Å and about 9 Å/mm at 5000 Å.

The monochromators are aligned by adjusting the optics so that all entrance slits are completely filled by the light beam, and are focused at the centerline of the

shock tube. The entrance slits are adjusted to focus at the shock tube centerline by using a light source at the monochromator exit slit.

The entire optical system, including the shock tube window and slit, is calibrated as one unit using a standard lamp located at the shock tube centerline. The calibration accuracy is limited by the statistical noise of the photomultiplier. To improve the signal to noise ratio, an ac calibration was made using a high speed light chopper. Two standard sources have been used: a tungsten ribbon filament lamp and a pyrometric carbon arc. The spectral intensity of the tungsten lamp was certified by Eppley Laboratory[2] by means of absolute calibration techniques developed by the National Bureau of Standards. In the ultraviolet region, a carbon arc has been used. Figure 20 presents the intensity distribution for the two calibration sources. Two tungsten lamp curves are shown. One lamp was calibrated at 35 amp to be used in the visible and near ultraviolet portions of the spectrum, and the other was calibrated at 30 amp to be used in the infrared. The true filament temperatures of the

[2]Personal communication from W. Scholar, The Eppley Laboratory, Inc., Scientific Instruments, Newport, Rhode Island, March 1963.

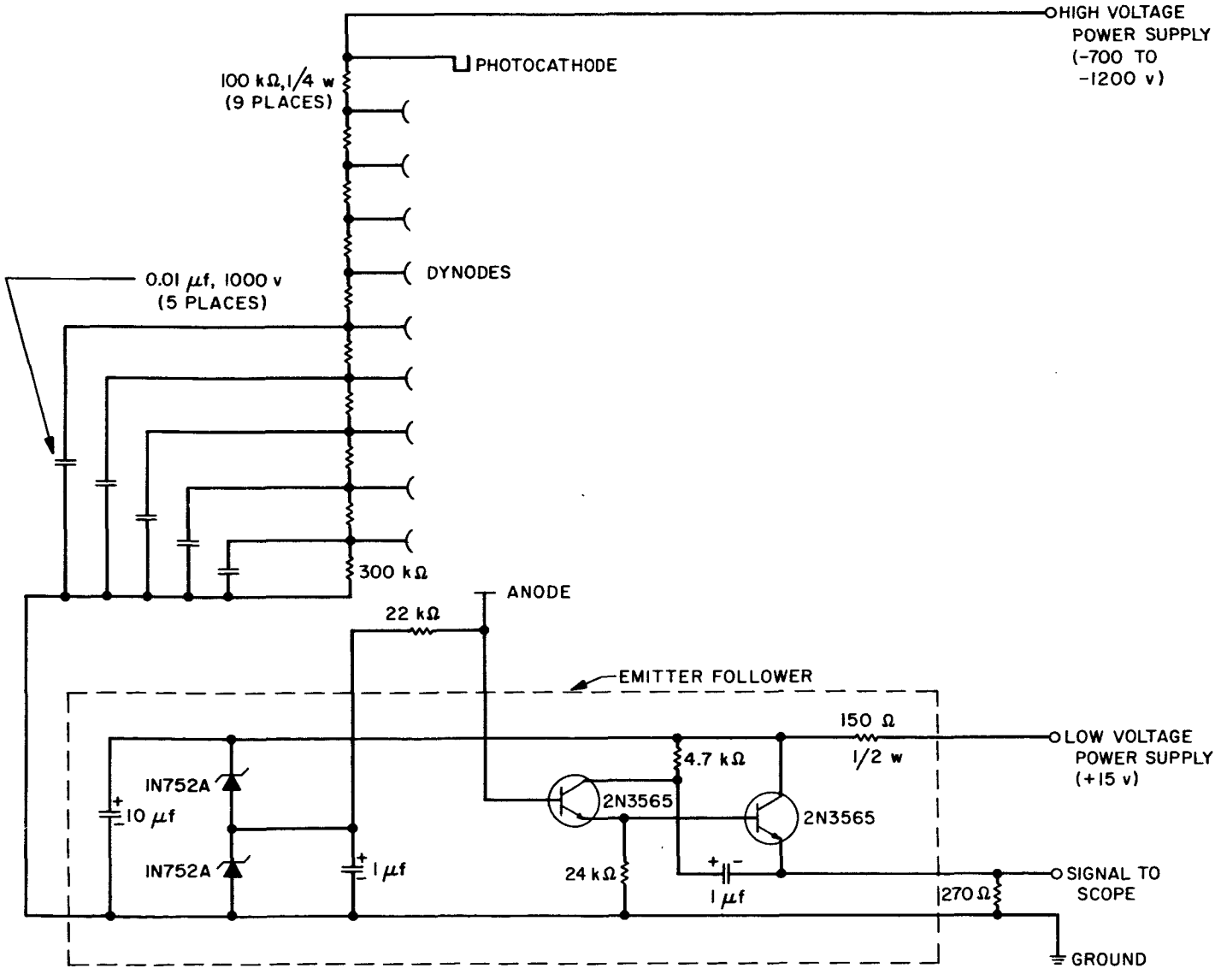

Fig. 18. RCA 1P28 photomultiplier circuitry. Emitter follower also used with other photomultipliers

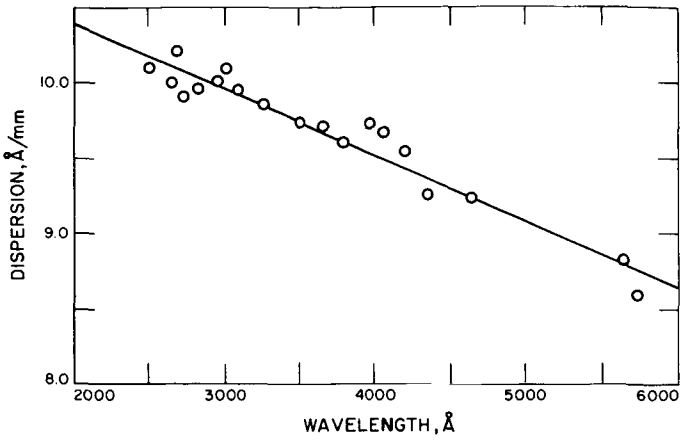

Fig. 19. Reciprocal linear dispersion in order I of the Jarrell–Ash grating spectrograph. Grating blazed for 5000 Å

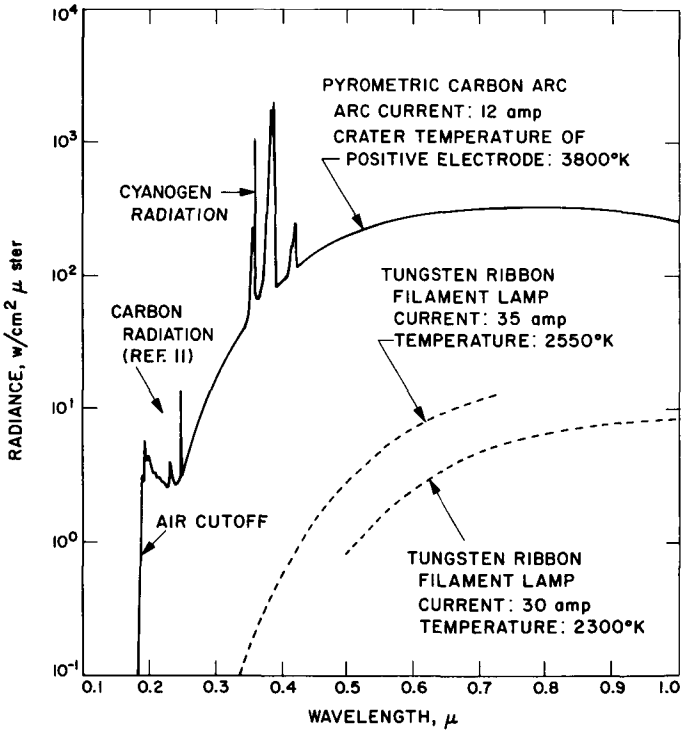

Fig. 20. Spectral radiance of typical carbon arc and tungsten lamp calibration sources

lamps are indicated on the figure. The carbon arc intensity is seen to be much higher over the entire spectrum than that of the tungsten lamp. With the exception of the C_2 and CN molecular bands, the arc intensity is a smooth function with wavelength. The carbon arc source is discussed further in Section III-D.

C. Data Reduction

If we assume that the gas radiation is isotropic, the radiant power (w/μ) entering the monochromator, for an optically thin gas, at wavelength λ is given by

$$P_g = \xi_\lambda G_\lambda \iiint d\Omega\, dA\, dx \tag{16}$$

and the power from the calibration lamp is

$$P_c = \xi_\lambda N_\lambda \iint d\Omega\, dA \tag{17}$$

where ξ_λ is a lumped parameter containing all transmission losses, monochromator efficiency, and detector sensitivity; G_λ is the specific intensity ($w/cm^3\ \mu$ ster) of the gas and N_λ is the intensity ($w/cm^2\ \mu$ ster) of the calibration lamp; and Ω is the solid angle, A is the cross sectional area of the field of view rays as defined by the optical arrangement, and x is the coordinate along the optical path.

For linear photomultipliers, the output voltage E is proportional to the input power P; thus, by ratioing (16) and (17) the specific intensity emitted by the gas is

$$G_\lambda = KN_\lambda \frac{E_g}{E_c} \tag{18}$$

where K is the view factor coefficient and is defined by

$$K = \frac{\iint d\Omega\, dA}{\iiint d\Omega\, dA\, dx} \tag{19}$$

The analytical solution of (19) is tedious for the optical arrangements of shock tube experiments, especially if all penumbra effects are considered. An alternate method is to determine the view factor coefficient experimentally. By integrating (17) over the path length L, one obtains

$$\int_0^L P_c\, dx = \xi_\lambda N_\lambda \iiint d\Omega\, dA\, dx \tag{20}$$

Combining (16) with (20) and assuming the power incident on the photomultiplier proportional to the output voltage, then

$$G_\lambda = N_\lambda \frac{E_g}{\int_0^L E_c\, dx} \tag{21}$$

The integral $\int_0^L E_c\, dx$ is obtained experimentally by moving the calibration lamp along the optical path and integrating a plot of the recorded outputs.

Equating (18) and (21), we obtain

$$K = \frac{E_c}{\int_0^L E_c\, dx} \tag{22}$$

Although E_c is a function of λ and x, K is only a function of x. To determine K for any convenient location of the calibration lamp, say x_i, the integral $\int_0^L E_c\, dx$ need only be measured once at any desired wavelength λ_0. Thus, at x_i

$$K(x_i) = \frac{E_c(\lambda_0, x_i)}{\int_0^L E_c(\lambda_0, x)dx}$$

To reduce data at other wavelengths requires only a plot of $E_c(x_i)$ vs λ. The measurements for the plot are obtained by placing the lamp at x_i and measuring the wavelength dependence of the output signal. The only restriction on x_i is that it be within the optical path. In our experiments, we have generally used the centerline of the shock tube where the image of the monochromator entrance slit is focused.

Typical data obtained from the monochromators is shown in Fig. 21. The nonequilibrium overshoot of species behind the shock wave is seen to occur in a fraction of a μsec. The radiation then decays to an equilibrium level, and the power to the monochromator remains constant until termination of the test by arrival of the driver gas. Typical measurements which have been made from these oscillograms are relaxation times, and the intensity of the nonequilibrium and equilibrium radiation.

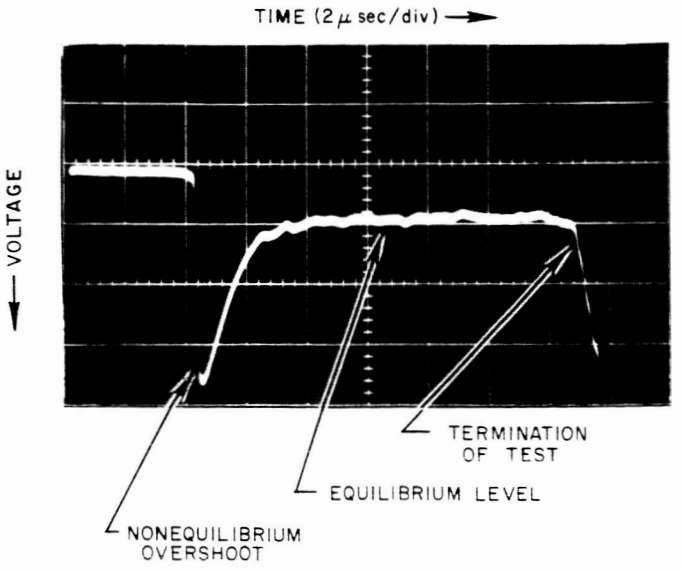

Fig. 21. Typical spectral radiation data. Data was obtained at λ = 5165 Å from a mixture of carbon dioxide, nitrogen, and argon. Shock speed was 25,600 ft/sec and initial pressure was 0.25 mm Hg

D. Carbon Arc Calibration Source

A well controlled carbon arc burning high-purity graphite rods is a reliable radiation standard (Ref. 7). Null and Lozier made a thorough study of the arc temperature, operating procedures, and intensity distribution across the crater of various grade spectroscopic rods (Ref. 8). They found that when operating the arc just under the overload current, the crater of the positive electrode radiates nearly as a 3800°K blackbody. Hankins developed an arc lamp (Ref. 9) which meets all requirements outlined by Null and Lozier. This type of lamp has been used at this laboratory to calibrate the monochromators.

The positive electrode is formed by a ¼-in.-dia Grade SPK graphite rod, and the negative electrode is formed by a ⅛-in.-dia Grade AGKS graphite rod. The electrodes are positioned at a 127° included angle and are continuously fed by two adjustable speed motors. When the calibrations were made only the central portion of the positive crater was focused on the monochromator entrance slit, thus insuring a uniform source intensity. The only spectral region where the calibration source does not radiate as a blackbody is the vicinity of the CN and C_2 molecular bands (see Fig. 20). These bands originate in the arc plasma which has a temperature of about 7000°K (Ref. 10) and dominates the solid carbon crater radiation. Spectrograms of the CN bands obtained with the Jarrell-Ash spectrograph are shown in Fig. 22. The plasma was viewed from the front, i.e., normal to the anode crater. The weak background luminosity seen on the spectrograms is radiation from the crater. The top spectrogram was obtained in order I using Polaroid 3000-speed film, a slit width of 10 μ, and an exposure time of 1/400 sec. The bottom spectrogram was obtained from order II using the same film but a slit width of 5 μ and an exposure time of 1/10 sec. The band-head vibrational transitions are identified along with their respective wavelengths. Much of the rotational line structure is seen in the spectrograms, particularly in order II.

In most spectrometric work where the carbon arc is used as a standard radiation source, the spectral regions containing the molecular bands are avoided. If the intensity distribution of these bands is known, however, the distribution may be integrated and used as a standard for low and moderate resolution work. Several experimenters have investigated the plasma radiation. Johnson

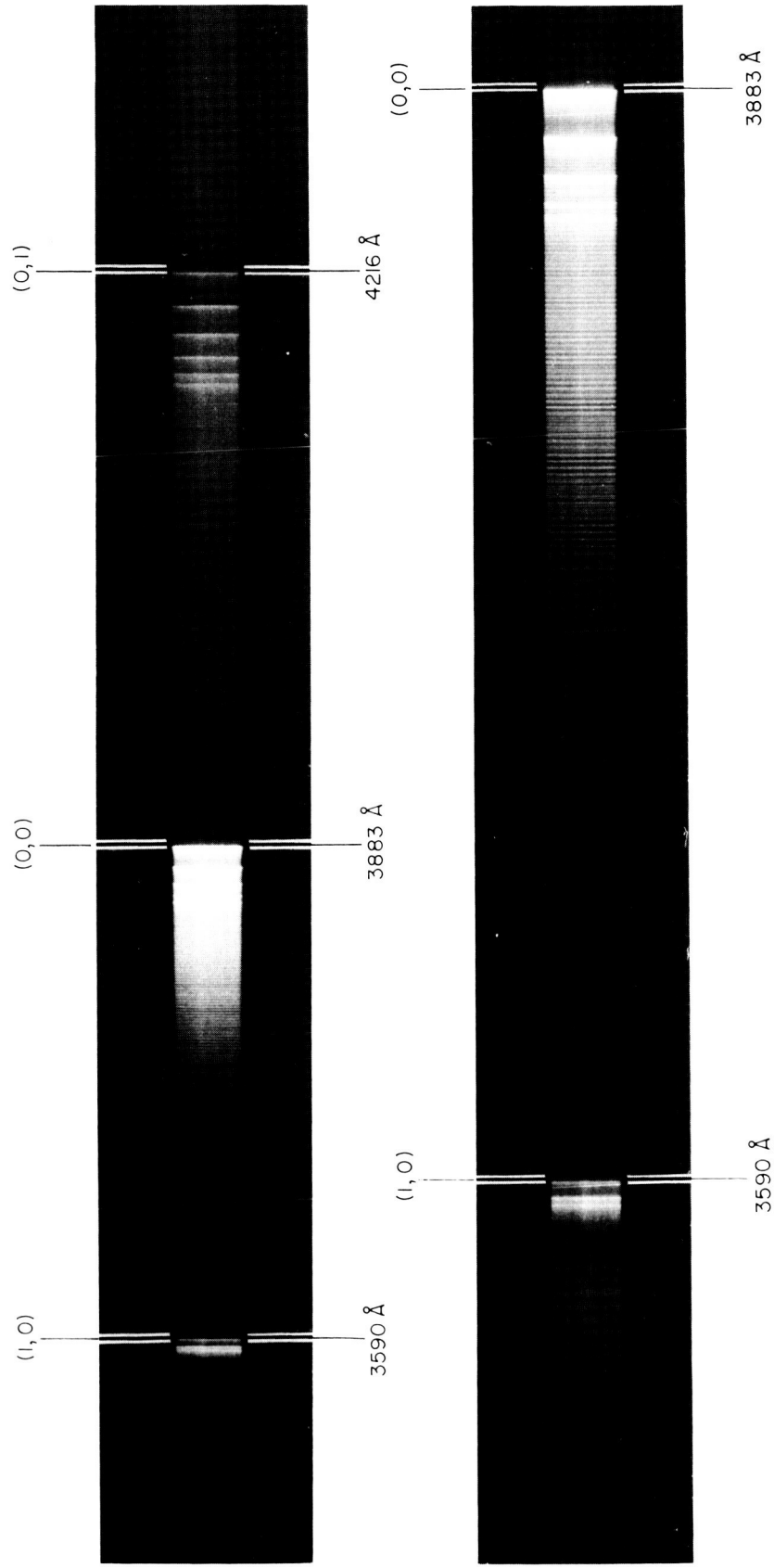

Fig. 22. Spectrograms of CN bands from the plasma of a carbon arc. Top spectrogram was obtained in order I and bottom obtained in order II

(Ref. 11) has studied the spectral intensity of the arc below 2500 Å in some detail. The integrated CN band intensity has been estimated by Euler (Ref. 12) and Null and Lozier (Ref. 8) to be 16 w/cm² ster and 6 w/cm² ster, respectively. Measurements by the authors with the Jarrell–Ash monochromator, already described, indicate an intensity contribution of 13.6 w/cm² ster from the CN bands. The band intensity was obtained by measuring an overall wavelength dependent "efficiency factor" for the monochromator and then using the efficiency factor to calculate the band intensity.

It was assumed that $E \sim R\tau N_\lambda \varepsilon$, where E is the photomultiplier output voltage, R is the photomultiplier response, τ is the transmission of any filters in the optical system, N_λ is the spectral intensity of the source (crater surface + plasma), and ε is the efficiency. For any two wavelengths the ratio of efficiency factors is

$$\frac{\varepsilon_2}{\varepsilon_1} = \frac{E_2}{E_1}\left(\frac{R_1}{R_2}\frac{N_{\lambda_1}}{N_{\lambda_2}}\frac{\tau_1}{\tau_2}\right) \tag{23}$$

By holding the monochromator slit sizes and the photomultiplier supply voltage constant, measurements of E were made from 2800–5400 Å. In portions of the spectrum, introduction of appropriate filters into the optical path was necessary to prevent photomultiplier saturation and to eliminate overlapping of order II. The spectral transmission τ of the filters was independently measured. The photomultiplier response was obtained from the manufacturer and the spectral intensity N_λ was calculated from Planck's equation for wavelengths on both sides of the CN bands. A plot of the data in the form $E/R\tau N_\lambda$ is presented in Fig. 23. The data has a maximum at 5000 Å, the blaze wavelength of the grating. A smooth curve was fitted to the data from which a normalized efficiency was obtained as follows

$$\frac{\varepsilon_\lambda}{\varepsilon_0} = \left(\frac{R\tau N_\lambda}{E}\right)_0 \left(\frac{E}{R\tau N_\lambda}\right)_\lambda \tag{24}$$

The subscript zero refers to conditions at $\lambda = 3300$ Å. Knowing the instrument efficiency made it possible to calculate the CN intensity from further photomultipler measurements as follows

$$N_\lambda = \frac{(E_\lambda/E_0)\,N_{\lambda_0}}{(\varepsilon_\lambda/\varepsilon_0)\,(R_\lambda/R_0)\,(\tau_\lambda/\tau_0)} \tag{25}$$

The results of these measurements are shown graphically in Fig. 24 and numerically in Table 1. A resolution of 5 Å was used to separate the major vibrational lines. The collective contribution of the rotational lines in the

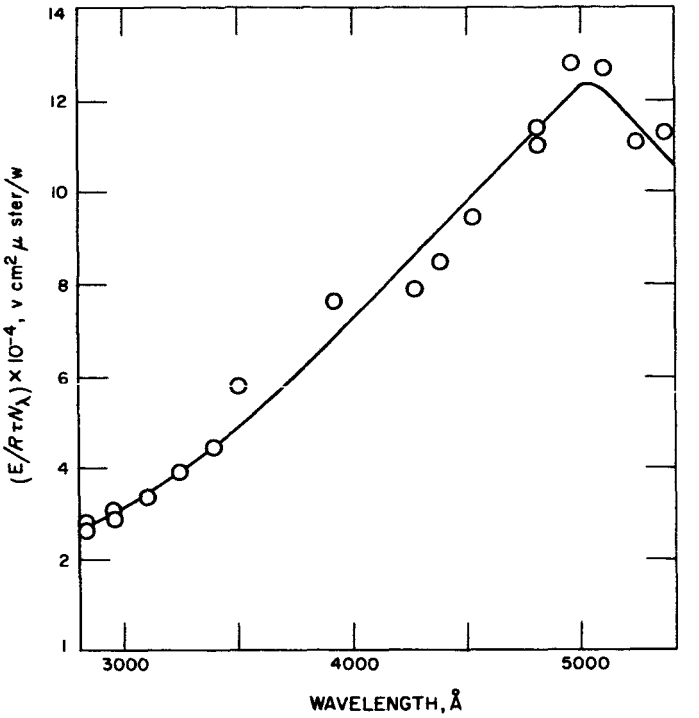

Fig. 23. Efficiency of monochromator used in determination of CN intensity from carbon arc calibration source

R-branches of the three bands forms a gradual falling off in intensity from the band heads. The blackbody curve plotted through the data is illustrative of the crater contribution to the total radiation from the arc in this region of the spectrum. It also shows good agreement with the data on both sides of the CN bands, which condition, of course, is necessary from the calculations. Around 4000 Å, the data falls below the blackbody curve but still remains within the estimated ±25% accuracy assigned to the measurements. The total CN intensity of 13.6 w/cm² ster already quoted was obtained by integrating the band area above the blackbody curve.

E. Stray Light Problems in the Ultraviolet

Stray light is a severe problem when working in the ultraviolet. Our experience has been that at wavelengths shorter than 2700 Å, visible stray light interferes significantly with the ultraviolet signal. By limiting the light from the monochromator entrance slit to a narrow beam falling on the grating surface, and by trapping the central image and undesired portions of the spectrum, we found that the stray light originated at the grating. Stray light of this nature comes from imperfections in the grating and occurs even in the most carefully prepared gratings.

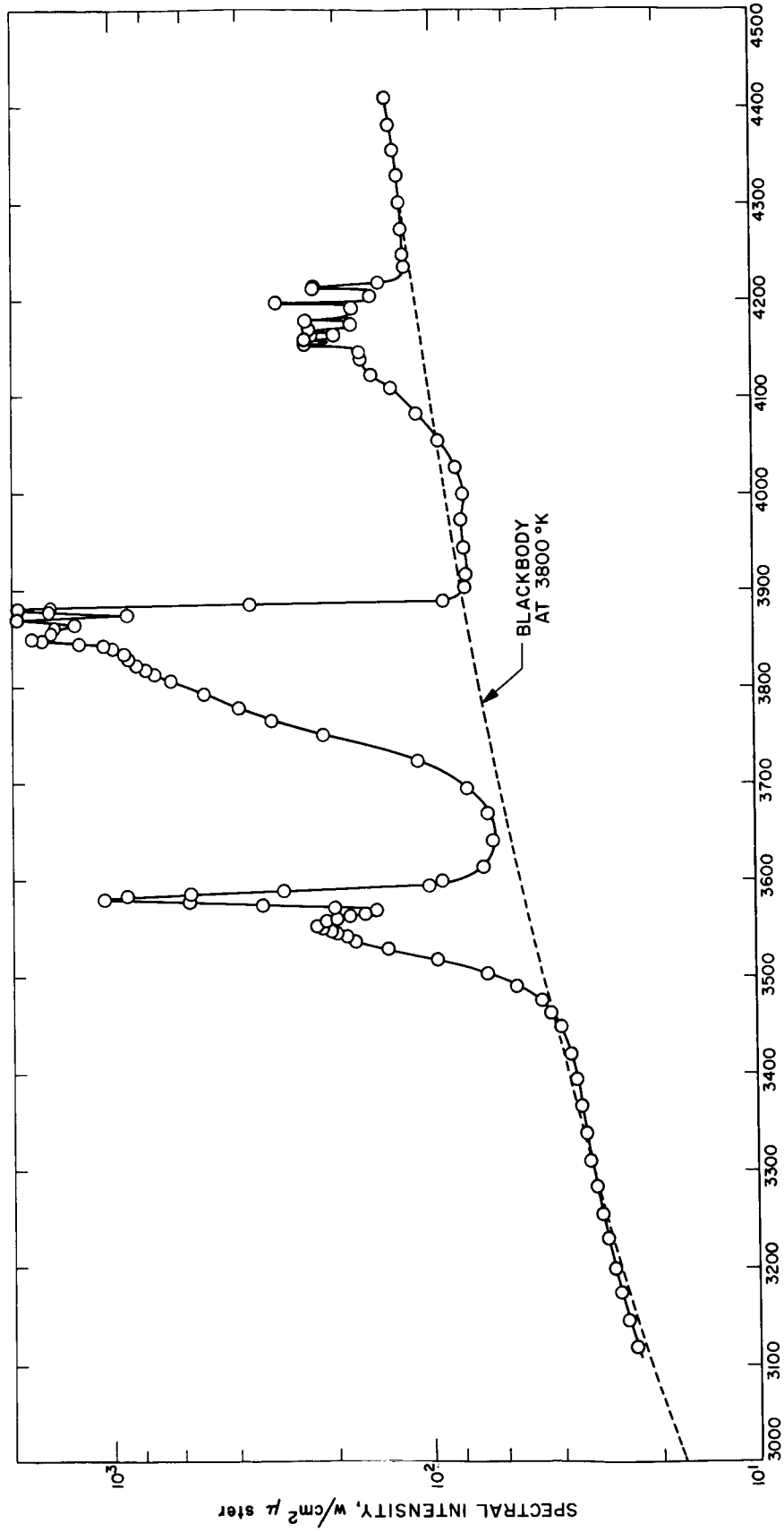

Fig. 24. CN radiation from carbon arc

Table 1. Spectral intensity of the carbon arc, including contributions from the incandescent anode and the arc plasma, in w/cm² μ ster

λ Å	Spectral intensity	λ Å	Spectral intensity	λ Å	Spectral intensity
4411	138	3883	1520	3581	1035
4383	136	3881	1980	3578	579
4356	130	3878	1560	3576	335
4329	127	3875	880	3573	199
4301	125	3871	2010	3570	147
4274	123	3865	1290	3567	159
4247	122	3862	1490	3565	178
4233	120	3857	1530	3562	197
4218	145	3854	1640	3559	210
4216	231	3851	1780	3554	226
4213	231	3848	1650	3551	217
4205	153	3846	1240	3549	202
4198	301	3843	1050	3546	193
4192	174	3841	976	3543	191
4180	244	3838	979	3538	172
4175	175	3835	897	3532	136
4169	234	3829	876	3518	95.2
4166	234	3823	828	3504	67.1
4164	199	3818	775	3491	54.9
4158	246	3813	724	3477	45.7
4153	246	3807	644	3463	42.9
4147	165	3793	508	3449	40.1
4137	164	3779	394	4322	37.5
4123	153	3766	312	3395	35.9
4109	133	3752	216	3367	34.8
4082	110	3724	110	3339	33.4
4054	94.4	3697	77.0	3311	32.8
4027	83.1	3670	66.5	3284	31.2
3999	79.3	3642	64.5	3256	30.2
3972	80.1	3615	68.6	3229	29.0
3945	78.1	3601	93.1	3200	27.8
3916	77.1	3596	103	3174	26.6
3903	77.6	3590	287	3146	25.2
3889	90.9	3587	561	3118	23.8
3886	365	3584	879		

A common approach for reducing the stray light intensity in the near ultraviolet has been to use a predispersing prism or grating. This may be accomplished by crossing two spectroscopes, the second one being the monochromator. The stray light is effectively reduced by this method, but at the sacrifice of useful signal intensity due to losses from the additional optics and path length.

Another method for reducing stray light is to use a filter that cuts out radiation of wavelength greater than 3000 Å. Unfortunately, filters possessing this quality do not have adequate transmission down to 2000 Å.

Still another method is to coat the window of the photomultiplier tube with sodium salicylate ($NaC_7H_5O_3$). Sodium salicylate is often used in ultraviolet work because of its high and relatively constant quantum yield characteristics (Refs. 13–17). In the usual application, a thin layer (2-4 mg/cm²) is applied to the photomultiplier tube window (which does not transmit UV radiation). As incident ultraviolet radiation passes through the coating, molecules are excited and visible fluorescence is observed. The visible fluorescence is then transmitted through the photomultiplier window to the detector. Knowing the quantum efficiency of the sodium salicylate makes it possible to calibrate the coated photomultiplier tube. Stray light of long wavelength does not cause fluorescence but is transmitted through thin coatings and acts directly on the photomultiplier. A thick coat should attenuate, by scattering, the specular transmission of stray light more than it does the fluorescent light, and so improve the stray light characteristics of the system (Ref. 11).

Coatings of various thicknesses were prepared by spraying a solution of sodium salicylate and methyl alcohol onto microscope slides with an airbrush. The slides were placed in front of the photomultiplier with the coated surface facing the incident radiation. The photomultiplier signal was recorded for λ between 2000 and 3000 Å. It was found that only with the thickest coating (7 mg/cm²) was there a noticeable reduction in stray light. The reduction was not sufficient for our purposes, however, and thicker layers are not feasible because they become flaky and nonuniform. In principle, the technique appears useful; but a better coating procedure than that used in these experiments is needed.

The stray light problem has been overcome by using a solar blind photomultiplier and a grating blazed for 3000 Å. The detector is an EMR Model 541F-05M. It has a cesium telluride cathode coated on the inside surface of a sapphire window. The quantum efficiency curve is nearly flat at 7% from 1800–2700 Å, then drops off rapidly to 0.01% at 3600 Å. Visible stray light does not fall within the response limits of the photomultiplier and its interference with ultraviolet measurements has, indeed, been found negligible.

IV. SUMMARY

Techniques for measuring spectral and total radiation in a hypervelocity shock tube have been developed. A carbon-coated thin film gage with μsec time response has been used to measure total stagnation point radiation. The spectral absorptance of the carbon coating was shown to vary not more than $\pm 20\%$ from 0.2 to 2.7 μ. A high signal to noise ratio for the gage was obtained, allowing the gage to be used over a wide range of heating rates. When the gage is used to study stagnation point radiation, it was pointed out that heating contributed from sources outside the bow shock can become important, depending upon the thermochemistry of the gas. A heat pulse technique was used for calibrating the total radiation gage. Shock standoff distances, needed to reduce total radiation data, have been measured by two independent methods.

By using commercially available monochromators and spectrographs, it has been shown how they can be adapted to the shock tube to make spectral radiation measurements. Spectral coverage from 2000–10,000 Å can be obtained by using various combinations of detectors and dispersing elements. Quantitative interpretation of the data was made possible by calibrating the entire optical system with standard light sources. The response time of the optical system was defined. The electrical response time was reduced by the addition of an emitter follower to the photomultiplier circuit. The data reduction procedure was outlined and the monochromatic gas intensity was shown to be directly proportional to the photomultiplier output signal. The carbon arc calibration source was studied and new measurements of the plasma CN radiance were obtained. The integrated CN radiation was found to contribute 13.6 w/cm^2 ster to the intensity of the carbon arc. Stray light problems were encountered between 2000 and 2700 Å. The stray light was found to originate at the grating face and to be of visible wavelength. Methods of eliminating the stray light were discussed.

NOMENCLATURE

A	area
c	heat capacity
E	voltage
$f(y)$	view factor for total radiation gage
G	intensity per unit path length, w/cm^2-cm
G_λ	specific intensity, w/cm^2 μ ster
H	absorptance
I	current
k	thermal conductivity
K	view factor coefficient
l	length of thin film gage
L	path length of radiating gas
N_λ	spectral intensity, w/cm^2 μ ster
P	spectral power, w/μ
q	heat transfer, w/cm^2
Q	constant heat input, w/cm^2
R	resistance, photomultiplier response
S	distance from radiating gas volume element to differential element of the gage
t	time
T	thickness, temperature
U_s	shock velocity
V	volume
W	width of thin film gage
x	coordinate along optical path
X	width of monochromator field of view in the shock tube
y	coordinate along thin film gage
α	temperature coefficient of resistance
β	thermal and material property of quartz
δ	shock standoff distance
ε	monochromator efficiency
θ	angle between line normal to gage surface and line from gage element to gas volume element
λ	wavelength
ξ	spectral instrument parameter
ρ	resistivity, density
τ	fractional transmission
ϕ	calibration constant
Ω	solid angle

NOMENCLATURE (Cont'd)

Subscripts

- c calibration
- g gage, gas
- i ith area element, ith position
- t total
- 0 initial conditions, reference conditions, normalized conditions at $\lambda = 3300$ Å
- 1 condition in front of incident shock wave
- 2 condition behind incident shock wave
- 3 condition at stagnation region of model

REFERENCES

1. Thomas, G. M., and Menard, W. A., "Experimental Measurement of Nonequilibrium and Equilibrium Radiation from Planetary Atmospheres," *AIAA Journal*, Vol. 4, No. 2, February, 1966, p. 227. Also available as Technical Report No. 32-902, Jet Propulsion Laboratory, Pasadena, California, April 1966.
2. Collins, D. J., Livingston, F. R., Babineaux, T. L., and Morgan, N. R., "Hypervelocity Shock Tube," Technical Report No. 32-620, Jet Propulsion Laboratory, Pasadena, California, June, 1964.
3. Thomas, G. M., and Menard, W. A., "Total Radiation Heat Transfer Gage for Hypervelocity Shock Tube Experiments," Technical Report No. 32-636, Jet Propulsion Laboratory, Pasadena, California, August, 1964.
4. Hewitt, E. W., "Description of the Aeromechanics Laboratory Heat Transfer Gage Calibration Unit," STL/TN-60-0000-19200, Space Technology Laboratories, Redondo Beach, California, November, 1960.
5. Camm, J. C., "High Speed Spectrograph Shutter," *Rev. Sci. Instr.*, Vol. 31, 1960, p. 278.
6. Vinokur, M., "Inviscid Hypersonic Flow Around Blunt Bodies," Tech. Note LMSD-48454, Lockheed Missiles and Space Company, Palo Alto, California, March, 1959.
7. MacPherson, H. G., "The Carbon Arc as a Radiation Standard," *Temperature, Its Measurement and Control in Science and Industry, 1*, Reinhold Publishing Corp., New York, 1941, p. 1141.
8. Null, M. R., and Lozier, W. W., "The Carbon Arc as a Radiation Standard," *Temperature, Its Measurement and Control in Science and Industry, 3*, Reinhold Publishing Corp., New York, 1962, p. 551.
9. Hankins, M. A., "The Pyrometric Molarc Radiation Standard at 3800°K," paper presented at the Second Annual Conference of the Temperature Measurements Society in Los Angeles, California, July, 1962.
10. Lochte-Holtgreven, W., "Production and Measurement of High Temperatures," *Reports on Progress in Physics, XXI*, The Physical Society, Great Britain, 1958, p. 312.
11. Johnson, F. S., "Spectral Radiance of the Carbon Arc from 1900 to 2500 Angstroms," *J. Opt. Soc. Am.*, Vol. 46, February, 1956, p. 101.

REFERENCES (Cont'd)

12. Euler, J., *Ann. Physik* (6), Vol. 11, 1953, p. 203.

13. Johnson, F. S., Watanabe, K., and Tousey, R., "Fluorescent Sensitized Photomultipliers for Heterochromatic Photometry in the Ultraviolet," *J. Opt. Soc. Am.*, Vol. 41, October, 1961, p. 702.

14. Watanabe, K., and Inn, E. C. Y., "Intensity Measurements in the Vacuum Ultraviolet," *J. Opt. Soc. Am.*, Vol. 43, January, 1953, p. 32.

15. Hammann, J. F., "Untersuchungen uber die Quantenausbeute von Leuchtstoffen unter Berucksichtigung ihrer Anwendung bei Strahlungsmessungen im UV," *Z. angew. Phys.*, Vol. 10, 1958, p. 187.

16. Allison, R., Burns, J., and Tuzzolino, A. J., "Absolute Fluorescent Quantum Efficiency of Sodium Salicylate," *J. Opt. Soc. Am.*, Vol. 54, June, 1964, p. 747.

17. Kristianpollar, N., "Absolute Quantum Yield of Sodium Salicylate," *J. Opt. Soc. Am.*, Vol. 54, October, 1964, p. 1285.

ACKNOWLEDGMENTS

The authors wish to thank two co-workers at Jet Propulsion Laboratory for their contribution to this work: C. L. Tuttle, for mechanical and optical instrumentation; and R. L. Hill, of the Instrumentation Section, for development of the electrical circuits.